^{1}H NMR Resonance Assignments, Secondary Structure, and Global Fold of Apo Bovine Calbindin D_{9k}[†]

Nicholas J. Skelton,[‡] Sture Forsén,[§] and Walter J. Chazin*,[‡]

Department of Molecular Biology, Research Institute of Scripps Clinic, La Jolla, California 92037, and Department of Physical Chemistry 2, Chemical Centre, University of Lund, S-221 00 Lund, Sweden

Received December 28, 1989; Revised Manuscript Received March 27, 1990

ABSTRACT: The solution structure and dynamics of apo bovine calbindin D_{9k} have been studied by a wide range of two-dimensional ^{1}H nuclear magnetic resonance experiments. Due to the presence of conformational heterogeneity in the wild-type protein, the sequential resonance assignment was carried out on a Pro43 → Gly mutant. By use of a combination of scalar correlation experiments acquired from H_2O solution, 61 of the 76 ^{1}H spin systems could be assigned to particular amino acid types. The remaining resonances were assigned by a parallel series of experiments acquired from ^2H_2O solution. These spin system assignments provided a basis for complete sequential resonance assignments from interresidue backbone nuclear Overhauser effects (NOEs). Elements of secondary structure were identified from sequential and medium-range NOEs, backbone spin–spin coupling constants, and slowly exchanging amide protons. Four sections of helix are delineated, together with a short antiparallel β-sheet interaction between the peptide loops involved in Ca^{2+} binding. The global fold is provided by combining these elements of secondary structure with a subset of the long-range, interhelix NOEs. Comparison with similar studies on the Ca^{2+}-saturated protein indicates that at this crude level the structures are very similar. However, removal of the Ca^{2+} does dramatically affect the dynamics of the protein, as judged by amide proton exchange rates and aromatic ring rotation. This is particularly evident in the increased flexibility of the residues in the hydrophobic core.

Calcium ions are involved in the regulation of many aspects of cell metabolism and function (Rasmussen, 1986a,b, 1989). External stimuli lead to transient increases in cytoplasmic Ca^{2+} concentration, these ions acting as a secondary messenger in the stimultion process. In many cases, the Ca^{2+} signal is translated by regulatory Ca^{2+}-binding proteins. The 10–100-fold increase in Ca^{2+} concentration (from the 10^{-7} M level in the resting cell) upon cell stimulation is sufficient to cause the regulatory sites in these proteins to bind calcium ions. It has been proposed that the binding of Ca^{2+} causes changes in the protein conformation that trigger further cellular responses (Ebashi et al., 1968; Cheung, 1970; Kakiuchi & Yamazaki, 1970).

The calmodulin superfamily of proteins exhibit a high degree of structural homology and represent a large proportion of the known Ca^{2+}-binding regualtory proteins. Four members of this family have been amenable to crystallization and analysis to high resolution by X-ray diffraction [parvalbumin (Moews & Kretsinger, 1975); calbindin D_{9k} (Szebenyi & Moffat, 1986); troponin C (Herzberg & James, 1988; Satyshur et al., 1988); calmodulin (Babu et al., 1988)]. These structures indicate that the Ca^{2+}-binding domains consist of a peptide loop, typically 12 residues long, flanked on either side by helix. This helix–loop–helix motif has been colloquially termed the "EF hand" (Kretsinger, 1972) or more recently the "calmodulin fold" (Krestinger, 1987). Further, it appears that it is not isolated EF hands but pairs of ion-binding sites which provide the basic functional unit (Seamon & Kretsinger, 1983). Interaction between binding sites (Vogel et al., 1985; Hofmann et al., 1988) and cooperative Ca^{2+} binding have been reported for calbindin D_{9k} (Linse et al., 1987).

The major deficiency of existing structural data on the Ca^{2+}-binding regulatory proteins is a lack of comparative high-resolution studies on the Ca^{2+}-saturated and apo forms of a single protein. Parvalbumin, calbindin D_{9k}, and calmodulin completely saturated with Ca^{2+} have been studied crystallographically, whereas troponin C has been studied with the N-terminal pair of EF hands free of metal ions. None of these molecules have been successfully crystallized in the complete absence of Ca^{2+}. Comparison of the N-terminal (apo) domain of troponin C with other Ca^{2+}-bound domains provides an indication, but does not allow an exact determination, of the structural *changes* occurring within a pair of EF hands as Ca^{2+} is bound (Herzberg et al., 1986). The obstacle caused by the crystallization requirement may be overcome by studying these proteins in solution with ^{1}H NMR.[1] Other solution methods, such as CD (Chiba et al., 1983a; Hennessey et al., 1987), UV (Dorrington et al., 1978), partial ^{1}H NMR assignments (Dalgarno et al., 1983; Ikura et al., 1985, 1987; Drakenberg et al., 1987), fluorescence (Chiba et al., 1983b; Chiba & Mohri, 1987), and low-angle X-ray scattering (Heidorn & Trewhella, 1988; Kataoka et al.,

[†] This work is supported by the National Institutes of Health (Grant GM 40120-01 to W.J.C.) and the Swedish Natural Science Research Council (operating grants to S.F.).

* To whom correspondence should be addressed.

[‡] Scripps Clinic.

[§] University of Lund.

[1] Abbreviations: CD, circular dichroism; UV, ultraviolet spectroscopy; r-calbindin, recombinantly expressed sequence of the minor A form of bovine calbindin D_{9k} (Fullmer & Wasserman, 1981) plus N-terminal methionine (Met0); P43G, r-calbindin with Pro43 replaced by Gly; NMR, nuclear magnetic resonance; 1D, one dimensional; 2D, two dimensional; COSY, correlated spectroscopy; R-COSY, relayed COSY; DR-COSY, double relayed COSY; MQ (2Q, 3Q), multiple (two, three) quantum spectroscopy; MQF-COSY (2QF-COSY, 3QF-COSY), multiple (two, three) quantum filtered COSY; NOE, nuclear Overhauser effect; NOESY, NOE spectroscopy; FID, free induction decay; 3-spin, $C^{\alpha}H$–$C^{\beta}H_2$ spin subsystem of serine, aspartic acid, asparagine, tyrosine, and phenylalanine residues; 5-spin, $C^{\alpha}H$–$C^{\beta}H_2$–$C^{\gamma}H_2$ spin subsystem of glutamic acid, glutamine, and methionine residues.

0006-2960/90/0429-5752$02.50/0

1989; Fujisawa et al., 1989), have been used to monitor structural effects associated with the binding of Ca^{2+}, but these techniques cannot provide site-specific information at an atomic level.

We have chosen to study calbindin D_{9k} by high-resolution ^1H NMR methods to investigate these conformational changes upon binding of Ca^{2+}. This protein is found predominantly in mammalian intestine cells and is thought to aid Ca^{2+} uptake in the intestine, or act as a Ca^{2+} buffer (Christakos et al., 1989). The protein has one archetypical EF hand, with 12 residues in the Ca^{2+}-binding loop, and a modified version of this motif containing a 14-residue loop (termed a pseudo EF hand). Thus, calbindin D_{9k} contains the pair of Ca^{2+}-binding domains common to the calmodulin superfamily but is sufficiently small (76 amino acids) that a complete assignment of resonances is possible by currently available ^1H NMR methods. This latter point is essential for an unambiguous determination of structure from ^1H NMR data. The gene for calbindin D_{9k} has been expressed in *Escherichia coli* (Brodin et al., 1986), allowing site-directed mutagenesis of the protein to further probe the influence of sequence on structure and dynamics.

The Ca^{2+}-saturated form of native calbindin D_{9k} and the site-specific mutant P43G (containing Pro43 replaced by Gly) have been studied by ^1H NMR, and complete resonance assignments have been made (Kördel et al., 1989, 1990). These studies revealed conformational heterogeneity in the native form of the protein, the conformer ratio being approximately 4:1. By assignment of all of the resonances observed in the spectrum, it was shown that the differences between the two forms arise from the Gly42–Pro43 peptide bond undergoing cis–trans isomerization (Chazin et al., 1989a). This was confirmed by observation of a single set of resonances for the P43G mutant. In the present study, we find that conformational heterogeneity is observed for apo wild-type r-calbindin D_{9k} but is absent for P43G. Structural characterization of Ca^{2+}-saturated *cis*-Pro43 and *trans*-Pro43 wild-type protein and the P43G mutant has shown that these three forms of calbindin D_{9k} are virtually identical (Kördel et al., 1990). The absence of conformational heterogeneity for the P43G mutant indicates that studies aimed at determination of the three-dimensional structures of apo and Ca^{2+}-saturated calbindin D_{9k} are best carried out on this mutant as opposed to the wild-type protein.

In this paper, we present the sequence-specific assignments for all backbone and side-chain ^1H NMR resonances of apo wild-type calbindin D_{9k} and apo P43G. On the basis of these assignments, elements of secondary structure have been identified, and the global folding pattern has been determined. The results for the apo protein are then compared with the solution (Kördel et al., 1989) and crystal structures (Szebenyi & Moffat, 1986) of Ca^{2+}-saturated calbindin D_{9k}.

Materials and Methods

The P43G mutant was prepared and purified as described previously (Brodin et al., 1986; Chazin et al., 1989b). Ca^{2+} was removed from the protein by titration with EDTA at pH 8.0 to a final molar ratio of 1:10 protein to EDTA. At this point the characteristic upfield-shifted methyl signals in one-dimensional ^1H NMR spectra indicated that the Ca^{2+} was no longer bound to the protein. The Ca^{2+}–EDTA complex and excess EDTA were then removed by ultrafiltration at 277 K using an Amicon 8 MC unit with a YM-2 membrane (M_r cutoff 2 kDa). The sample volume was reduced from 2.0 to 0.5 mL with a 3-atm excess pressure of argon. This process was repeated six times, and the final solution was lyophilized. The protein samples were then dissolved in 0.42 mL of ^1H_2O, containing 5% (v/v) ^2H_2O for the spectrometer lock circuitry (for brevity referred to as H_2O solution), or "100%" ^2H_2O (Merck Isotopes, Montreal, Canada) to a final protein concentration of 4–5 mM. The pH was adjusted to 5.3 by addition of microliter amounts of 0.01 M NaOH, HCl, NaO^2H, or ^2HCl. The ^2H_2O samples were prepared under argon, and pH* was not corrected for isotope effects.

All NMR experiments were performed on Bruker AM-500 and AM-600 spectrometers equipped with Aspect 3000 computers and digital phase shifting hardware. The temperature was 300 K unless indicated otherwise. Standard pulse sequences and phase cycling were utilized to obtain phase-sensitive COSY (Marion & Wüthrich, 1983) and R-COSY and DR-COSY (Wagner, 1983a) experiments in H_2O solution and to obtain 2QF-COSY and 3QF-COSY (Rance et al., 1983; Rance & Wright, 1986) experiments in ^2H_2O solution. The delays for R-COSY (τ = 40 ms) and DR-COSY (τ_1 = 22 ms, τ_2 = 40 ms) were optimized according to Chazin and Wüthrich (1987). 2Q (τ = 30 ms) and 3Q (τ = 22 ms) experiments were performed with the pulse sequence and phase cycling described by Braunschweiler et al. (1983), with a composite 180° pulse (Levitt & Freeman, 1979). Pure absorption NOESY (τ_m = 200 ms) spectra were acquired with the normal pulse sequence (Macura & Ernst, 1980; Kumar et al., 1980) followed by a short Hahn-echo period to improve the quality of the base line [for example, see Davis (1989)]. Minimum phase cycling of the 90° pulses (Bodenhausen et al., 1984) was used along with phase alteration of the 180° echo pulse. NOESY spectra were also acquired without presaturation by use of a jump–return observation pulse (Plateau & Guéron, 1982). Pure absorption TOCSY experiments (τ_m = 50, 70, or 110 ms; Cavanagh et al., 1990) were obtained according to the modification described by Rance (1987), with a Hahn-echo period as described for the NOESY experiment.

All spectra were recorded in the phase-sensitive mode. Quadrature detection in the ω_1 dimension was achieved by use of time-proportional phase incrementation (Marion & Wüthrich, 1983). The carrier was set on the solvent resonance for experiments acquired from H_2O solution. For the ^2H_2O TOCSY, MQ, and MQF experiments the carrier was set just downfield of the $C^\alpha H$ resonances, and the spectra folded about this point in ω_1. The transmitter frequency was moved to the center of the aliphatic spectrum during the spin-locking period of the ^2H_2O TOCSY experiments. A preacquisition delay of 1.2–1.4 s was used, during which time the solvent resonance was routinely attenuated by coherent low-power irradiation. The solvent irradiation during the ^2H_2O experiments was gated off 100–200 ms prior to the start of the pulse sequence. Solvent irradiation was also carried out during the mixing time of NOESY spectra acquired in H_2O but not during the mixing periods of any other experiments. Typically, a total of 2048 quadrature pairs of data points were collected over 6250 Hz in the sequential acquisition mode for each t_1 value. COSY and MQF-COSY spectra were recorded with t_{1max} ranging from 70 to 90 ms, while R-COSY, DR-COSY, MQ, TOCSY, and NOESY spectra were acquired with t_{1max} ranging from 35 to 45 ms.

The raw data were processed either on an Aspect 3000 data station using Bruker software or on a Convex C240 computer with the FTNMR program provided by Dr. Dennis Hare, modified for use on the Convex by Duane Waliser. Application of window functions and base-line corrections were performed as described in Chazin et al. (1988). Experiments that are cosine modulated in the ω_1 dimension were routinely

treated for suppression of t_1 ridges by halving the intensity of the first free induction decay (Otting et al., 1985). The final data matrix was usually 1024 real points in ω_1 and 2048 real points in ω_2, giving a digital resolution of 4.6 and 2.9 Hz/point, respectively.

Slowly exchanging protons were identified by acquiring NOESY spectra in H_2O solution on protein in which all amide hydrogens had been previously exchanged in ^2H_2O. Two 7-h NOESY spectra were recorded: the first at 278 K, 3 h after sample dissolution, and the second at 290 K, started after the sample had been kept at 278 K for 20 h and at 290 K for 6 h. Hydrogens are described as rapidly exchanging if they exhibited NOEs in both spectra, slowly exchanging if they exhibited NOEs in only the second spectrum, and very slowly exchanging if no NOEs were observed.

Backbone coupling constants ($^3J_{NH\alpha}$) were measured from ω_2 cross sections (Marion & Wüthrich, 1983) through peaks in the H_2O COSY spectrum (t_{1max} = 90 ms) processed with an unshifted sine bell in ω_2 and zero filled to a final digital resolution of 2.2 Hz/point in ω_1 and 0.4 Hz/point in ω_2.

Results

The sequence-specific assignments were obtained first for the apo form of P43G, because this mutant does not exhibit conformational heterogeneity. Spectra have also been acquired on the apo form of the wild-type protein and carefully compared with those of P43G. Assignments for the major (*trans*-Pro43) isoform of the wild-type protein could be obtained directly from those for P43G. In general, the chemical shifts and the pattern and intensities of NOEs are identical for the wild-type and mutant proteins, except for the residues adjacent to position 43. These results imply that apo P43G is virtually identical with the apo form of calbindin D_{9k}. The spectra of apo wild-type protein also contain resonances of a second species which we attribute to the minor (*cis*-Pro43) isoform. Integration of peaks in the 2D spectra indicate that the ratio of the two isoforms is approximately 4:1 (similar to that observed for Ca^{2+}-saturated calbindin D_{9k}). Thus, removal of the Ca^{2+} from the protein does not affect the thermodynamics of the proline cis–trans isomerization.

Sequential Assignment Strategy. The procedure used to obtain the sequence-specific ^1H NMR resonance assignments was developed by Wüthrich and co-workers [reviewed in Wüthrich (1986)]. Amino acid spin systems were identified by the integrated strategy described in Chazin et al. (1988). A strong emphasis was placed on scalar correlation experiments acquired from H_2O solution, with the aim of observing relayed connectivities from the side-chain protons to the backbone amide proton [discussed in Chazin and Wright (1987)]. Scalar correlation experiments acquired in ^2H_2O were required to completely characterize some of the longer side chains. MQ and MQF-COSY experiments provided complete side-chain assignments, reliably discriminating between proton positions along the side chain and providing evidence for resonance degeneracy within the same side chain. Characteristic through-space (NOE) connectivities between aromatic or side-chain amide protons and backbone proton resonances allowed all of the phenylalanine, tyrosine, and asparagine and half of the glutamine spin systems to be distinguished. The spin systems classified with the correlation spectra provided an ample basis for sequence-specific assignment by the standard protocol of Billeter et al. (1982).

Spin System Identification. (A) Preliminary Analysis of Fingerprint Regions. For a protein of 76 residues, including 3 prolines, cross-peaks from 72 residues should be observable in the backbone fingerprint region (ω_1 = $C^\alpha H$, ω_2 = NH) of the COSY spectrum. For P43G, cross-peaks from only 69 residues are observed (Figure 1). The 2Q spectrum contained two further NH–$C^\alpha H$ correlations, Asp58 and Ser2, whose COSY cross-peaks were attenuated by the solvent irradiation because their $C^\alpha H$ frequencies were close to that of the H_2O signal. The $C^\alpha H$ proton of the final residue (Ser24) was found to lie exactly under the H_2O resonance at this temperature and pH; correlations to it were only observed by lowering of the temperature to 290 K.

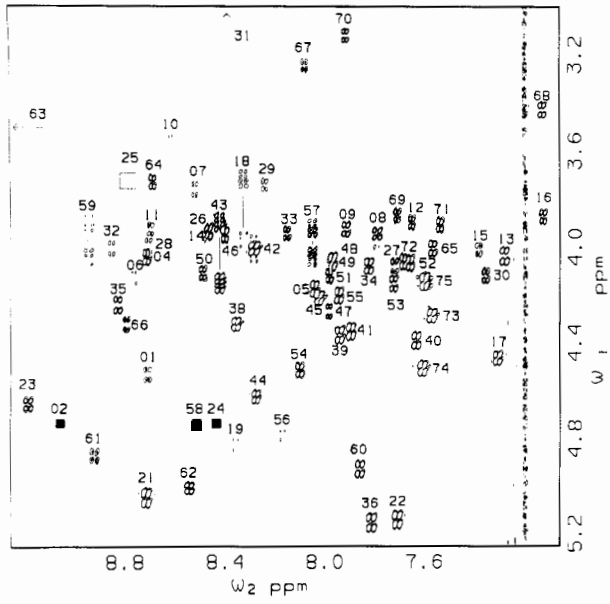

FIGURE 1: Backbone fingerprint region of a 500-MHz COSY spectrum of 4 mM P43G at 300 K and pH 5.3. The ω_1 = $C^\alpha H$, ω_2 = NH cross-peaks are labeled with the sequence-specific assignments. Arrows indicate cross-peaks that appear outside the region shown. The filled boxes represent correlations that are missing from this spectrum due to $C^\alpha H$ saturation during solvent suppression but were observed in other spectra acquired at 300 or 290 K. Empty boxes indicate the location of correlations observed only at lower contour levels.

Both alanine $C^\alpha H$–$C^\beta H_3$ cross-peaks could be readily identified in the characteristic upfield region of the COSY spectrum. However, only a single, distorted threonine $C^\beta H$–$C^\gamma H_3$ cross-peak was discernible. The subsequent analysis of the DR-COSY spectrum indicated that Thr34 and Thr45 have nearly identical chemical shifts for both $C^\beta H$ and $C^\gamma H_3$. Of the 32 methyl doublet resonances expected from the 3 valine, 12 leucine, and 2 isoleucine residues, only 31 could be identified in the COSY spectrum (see Figure 2). It later became evident that the absence of one cross-peak was due to the degeneracy of the $C^\delta H_3$ protons of Leu39. Correlations to the $C^\delta H_3$ groups of the two isoleucines were readily identified by virtue of their triplet cross-peak fine structure.

The tyrosine and three of the five phenylalanine ring spin systems were readily identified in the downfield region of the COSY spectrum. The other two phenylalanine ring systems were identified by analysis of 2Q and 3Q spectra. 3Q frequencies at ($C^\delta H$ + $C^\epsilon H$ + $C^\zeta H$) and ($C^\epsilon H$ + $C^\zeta H$ + $C^{\epsilon'} H$) were observed for all five phenylalanine rings. The cross-peaks due to scalar couplings between pairs of side-chain amide protons of the six asparagine and glutamine residues were also observed in these regions of the COSY and 2Q spectra.

The successful location of the requisite number of NH–$C^\alpha H$, methyl group, and aromatic ring spin systems indicates two important points about this sample. First, as was found for the Ca^{2+}-saturated state, the Pro43 → Gly mutation removes all signs of the conformational heterogeneity present in the native protein, greatly simplifying the task of complete resonance assignment (Kördel et al., 1990). Second, the presence

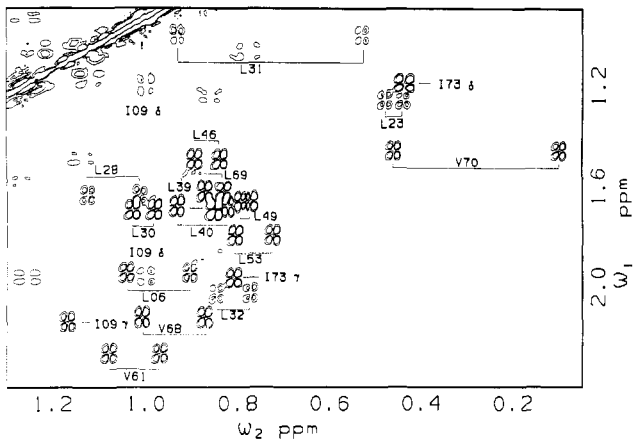

FIGURE 2: Valine/leucine/isoleucine fingerprint region of a 600-MHz DQF-COSY spectrum of 3 mM P43G in ^2H_2O at 300 K and pH* 5.3. The valine (ω_1 = $C^\beta H$, ω_2 = $C^\gamma H_3$), leucine (ω_1 = $C^\gamma H$, ω_2 = $C^\delta H_3$), and isoleucine (ω_1 = $C^\beta H$, ω_2 = $C^\gamma H_3$ and ω_1 = $C^\gamma H_2$, ω_2 = $C^\gamma H_3$, identified as γ and δ, respectively) cross-peaks are labeled with their sequence-specific assignments.

of a single set of resonances verifies that the Ca^{2+} has been completely removed from the protein. By studying the upfield-shifted methyl resonances in 1D ^1H NMR spectra, we deduce that the samples in these studies contained less than 0.5% of the Ca^{2+}-saturated protein. In some of the initial samples that we studied, there was contamination with a small amount of Ca^{2+} leading to extra resonances in the spectra and chemical exchange peaks in TOCSY and NOESY experiments. The exchange cross-peaks indicate that the calcium ions transfer between protein molecules on a time scale of 0.1–10 s and suggests that ^1H NMR can be used to study the kinetics of Ca^{2+} binding.

(B) Identification of Backbone Amide Based Spin Systems. A substantial number of the side-chain protons could be related to their backbone amide protons by the direct and relayed connectivities present in the COSY, 2Q, R-COSY, DR-COSY, and TOCSY spectra acquired from H_2O solution. The delays in the DR-COSY were optimized to obtain correlations at ω_1 = $C^\beta H$, ω_2 = NH (Chazin & Wüthrich, 1987), and this experiment was successful in locating 93 of the 123 $C^\beta H$ resonances in the protein. Inclusion of the TOCSY data raised this figure to 111. All of the $C^\beta H_2$ groups identified from relayed connectivities were subsequently verified by at least one of the following: $C^\alpha H$–$C^\beta H$ correlations in 3QF-COSY; remote peaks ($\omega_1 = \omega_\beta + \omega_{\beta'}$, $\omega_2 = \omega_\alpha$) in 2Q spectra; direct peaks ($\omega_1 = \omega_\alpha + \omega_\beta + \omega_{\beta'}$, $\omega_2 = \omega_\alpha, \omega_\beta, \omega_{\beta'}$) in 3Q spectra. The TOCSY spectra also permitted the identification of some 71 of the 86 $C^\gamma H$ resonances. The H_2O correlation spectra located a sufficiently high number of side-chain protons that 67 of the spin systems could be assigned to residue type on the basis of coupling patterns and chemical shifts.

(C) Assignment of Residues with Unique Spin Systems. Although four glycine residues were identified directly in the COSY spectrum, the complete assignment of all six glycine residues was most readily obtained from remote peaks at $\omega_1 = \omega_\alpha + \omega_{\alpha'}$ and $\omega_2 = \omega_{NH}$ in the 2Q spectrum. The combined data from R-COSY and DR-COSY spectra permitted all side-chain protons of the threonine, alanine, and valine residues to be correlated with the corresponding backbone amide proton.

For 9 of the 12 leucine and both isoleucine residues, the methyl-based spin subsystems identified in the COSY spectrum were correlated to their backbone resonances from connectivities between NH and $C^\delta H_3$ in TOCSY spectra. The lack of coherence transfer to the amide proton from the $C^\delta H_3$ for Leu28, Leu31, and Leu32 is due to small scalar couplings between backbone NH and $C^\alpha H$. The correlation of side-chain protons to the backbone protons for these three remaining leucine residues was established from $C^\alpha H$–$C^\delta H_3$ connectivities observed in TOCSY spectra. Remote peaks ($\omega_1 = \omega_\gamma + \omega_{\gamma'}$, $\omega_2 = \omega_\delta$) in the 2Q spectrum indicated that the $C^\gamma H_2$ protons of Ile73 were degenerate.

The key characteristic for the identification of the lysine spin systems is the unique $C^\epsilon H_2$ chemical shift. Seven of the ten lysine backbone spin systems could be distinguished by relayed connectivities from $C^\epsilon H_2$ to the amide proton in TOCSY spectra. The correlation of side-chain to backbone protons for the three other spin systems was established from $C^\alpha H$–$C^\epsilon H$ connectivities. 2Q, 3QF-COSY, and 3Q spectra were used to assign unambiguously resonance positions to specific protons along the side-chain and to verify instances of resonance degeneracy (Chazin et al., 1987). Resonance degeneracy could not be proven for the $C^\gamma H_2$ protons of Lys7, Lys25, and Lys72 but was assumed due to the lack of unassigned correlations in the TOCSY spectra and the near degeneracy of other methylene resonances along the side chain.

(D) Assignment of Residues with 3-Spin and 5-Spin Side Chains. A total of 14 of the 18 residues with 3-spin side chains were completely identified from connectivities to the backbone amide proton in the TOCSY or DR-COSY experiments. The resonance assignments for the other four spin systems were made from $C^\alpha H$–$C^\beta H$ connectivities in MQ and MQF-COSY spectra. The 3-spin spin systems were further classified to specific amino acids by intraresidue NOEs from aromatic rings (phenylalanine and tyrosine) or side-chain amide protons (asparagine) to backbone amide, C^α, and/or C^β protons. The C^β chemical shifts proved sufficient to locate the serine residues; in all cases these were the only 3-spin spin systems to have $\delta(C^\beta H) > 3.80$ ppm. By elimination, the four remaining 3-spin spin systems were attributed to the four aspartic acid residues.

The observation of four distinct side-chain resonances relayed to the backbone amide proton allowed 11 of the 17 5-spin spin systems (this excludes Met0, which is discussed below) to be identified in DR-COSY and TOCSY spectra. Only three distinct relayed connectivities could be identified for the other 5-spin spin systems. For Glu27, four distinct side-chain resonance positions were identified from relayed connectivities to the C^α proton. For Glu52 and Gln67, remote peaks in the ^2H_2O 2Q spectrum at $\omega_1 = \omega_\beta + \omega_{\beta'}$, $\omega_2 = \omega_\alpha$ showed that the absence of relayed connectivities was due to the degeneracy of the $C^\beta H$ resonances. For Glu48, Glu65, and Gln75 two distinct $C^\beta H$ resonances were unambiguously assigned from 2Q spectra, and resonance degeneracy of the C^γ protons was assumed but could not be proven. In general, the side-chain amide groups of the glutamine residues displayed only weak NOEs to other side-chain protons. Consequently, only two out of the four spin systems (Gln33 and Gln67) could be directly identified.

(E) Identification of the N-Terminal Methionine and Proline Spin Systems. The spin systems of the N-terminal methionine (Met0) and the proline residues were entirely assigned after all other spin systems had been identified in the ^2H_2O spectra; only four C^α-based spin systems were unassigned at this stage of the analysis. The $C^\alpha H$–$C^\beta H_2$ assignments were made in the MQF-COSY and MQ spectra. The remaining resonance positions were identified from relayed connectivities to $C^\alpha H$ or proline $C^\delta H_2$ in the TOCSY spectra.

For Met0, the degeneracy of the $C^\gamma H$ protons could be explicitly identified from the presence of a remote peak in the

3Q spectrum at $\omega_1 = \omega_\gamma + \omega_{\gamma'} + \omega_\beta$, $\omega_2 = \omega_{\beta'}$. The narrow singlet methyl signal at 2.05 ppm in the 1D spectrum is attributed to Met0 even though no intraresidue NOEs are present to corroborate this. For Pro20, the direct peaks in the 3Q spectrum at $\omega_1 = \omega_\delta + \omega_{\delta'} + \omega_\gamma$ and $\omega_1 = \omega_\delta + \omega_{\delta'} + \omega_{\gamma'}$ are crucial to the assignment, showing the magnetic equivalence of the C^δ protons and the resonance degeneracy of one C^β with one C^γ proton. Similarly, remote peaks in 2Q ($\omega_1 = \omega_\beta + \omega_{\beta'}$, $\omega_2 = \omega_\alpha$) and 3Q ($\omega_1 = \omega_\gamma + \omega_{\gamma'} + \omega_\delta$, $\omega_2 = \omega_{\alpha''}$) spectra show that the C^γ protons of Pro37 are magnetically equivalent and also degenerate with one of the C^β proton resonances. For Pro3, connectivities are not observed between the $C^\delta H_2$ group and the rest of the residue. The correlation of the two portions of the spin system was established on the basis of sequential NOEs from Ser2 $C^\alpha H$ to Pro3 $C^\delta H_2$ and from Pro3 $C^\alpha H$ to Glu4 NH.

At the end of the spin system identification procedure 61 spin systems (all of the Gly, Ala, Val, Leu, Ile, Pro, Thr, Lys, Ser, Phe, Tyr, Asn, and Asp and two of the four Gln) had been specifically assigned to the appropriate amino acid. The remaining 15 were glutamic acid or glutamine residues.

Sequence-Specific Assignments. The sequence-specific assignments were obtained according to the standard sequential assignment procedure of Billeter et al. (1982) and are listed in Table I. The short-hand notation of Wüthrich et al. (1984) is adopted for specifying short proton–proton distances and the corresponding NOEs. We estimate that, under the conditions of these experiments, NOE cross-peaks are observed between protons up to 5.5 Å apart and that some correlations are affected by a limited amount of spin diffusion.

The sequence-specific assignments for residues in helical conformation were most easily obtained from the d_{NN} NOEs, although in most cases these were also confirmed by the presence of less intense $d_{\alpha N}$ connectivities. Two sections from a NOESY spectrum are depicted in Figure 3, showing the d_{NN} connectivities in the regions subsequently defined as helix. For regions of polypeptide in an extended conformation, strong $d_{\alpha N}$ NOEs provide the primary means of assignment (data not shown). Figure 4 contains a summary of the d_{NN}, $d_{\alpha N}$, and $d_{\beta N}$ connectivities observed in apo P43G. As indicated in the figure, the majority of the sequential assignments could be made from a single NOESY spectrum (τ_m = 200 ms) obtained at 300 K. However, due to the base-line distortion about ω_1 = 4.75 ppm (arising from the residual H_2O peak), not all $d_{\alpha N}$ connectivities were discernible under these conditions. This problem was alleviated by acquiring a NOESY spectrum with a jump-return observation pulse. The remaining assignment gap in the center of the third helix was resolved by the $d_{\alpha N}(i,i+3)$ medium-range NOE from Asp47–Phe50. However, there remained ambiguity for two 5-spin spin systems with backbone amide chemical shifts of 7.96 and 7.57 ppm that were assigned by default to Glu48 and Gln75. For both of these spin systems, we made the unusual observation that no sequential NOEs could be found. This is attributed to backbone amide degeneracy of consecutive residues, which would preclude the observation of the sequential NOEs. The complete absence of sequential NOEs between the three spin systems at ~7.97 ppm and the two at ~7.60 ppm is only consistent with Asp47, Glu48, and Leu49 all having nearly coincident backbone amide chemical shifts (7.98, 7.96, and 7.97 ppm, respectively), with a similar situation arising for Ser74 and Gln75 (7.61 and 7.60 ppm, respectively).

Secondary Structure. The data obtained from the NMR spectra enable the elements of secondary structure to be located, notably helix and extended peptide. As reviewed in

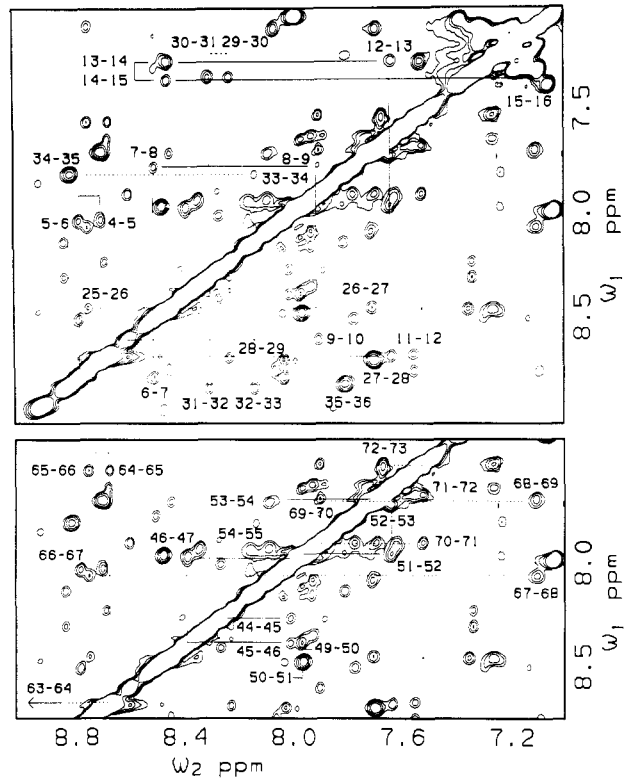

FIGURE 3: Region of a 500-MHz Hahn-echo NOESY spectrum (τ_m = 200 ms) of 4 mM P43G at 300 K and pH 5.3. Sequential d_{NN} NOEs are indicated for polypeptide segments in helical conformation. The numbers adjacent to the cross-peaks indicate the residues involved in the sequential connectivity. The data for helix I (Glu4–Lys16, solid line) and helix II (Lys25–Phe36, broken line) are identified in the upper panel. The data for helix III (Ser44–Lys55, solid lines) and helix IV (Phe63–Ser74, broken line) are identified in the lower panel. Not all of the sequential NOEs for Asp47, Glu48, Leu49, and Glu51 can be observed because their backbone amide resonances are degenerate (see text).

Wüthrich (1986), helical regions are strongly suggested by continuous sections of intense sequential d_{NN} connectivites and are confirmed by the observation of medium-range NOEs [$d_{\alpha N}/d_{NN}(i,i+2)$, $d_{\alpha\beta}/d_{\alpha N}(i,i+3)$, and $d_{\alpha N}(i,i+4)$], small scalar coupling constants ($^3J_{NH\alpha}$ < 6 Hz), and slow amide proton exchange rates. Sequential NOEs, backbone coupling constants, and slowly exchanging amides are shown in Figure 4. The medium-range NOE data have been presented in a preliminary communication (Skelton et al., 1990). Helices extend over the following regions, in complete agreement with the helices assigned in our earlier work: Ser2–Lys16 (helix I), Ser24–Glu35 (helix II), Ser44–Lys55 (helix III), and Phe63–Ser74 (helix IV). The extent of these helices in the apo protein is very similar to that observed in the NMR (Kördel et al., 1989) and crystallographic (Szebenyi & Moffat, 1986) studies of the Ca^{2+}-saturated calbindin D_{9k}.

Regions of peptide in extended conformation are evidenced by intense sequential $d_{\alpha N}$ NOEs, large coupling constants ($^3J_{NH\alpha}$ > 8 Hz), and weak or unobservable d_{NN} and intraresidue $d_{N\alpha}$ NOEs. Residues Gln22-Leu23-Ser24 and Glu60-Val61-Ser62-Phe63 fit these criteria, and the long-range NOEs between these two strands indicate an antiparallel β-sheet arrangement (Skelton et al., 1990). This "mini-β-sheet" is also observed in both crystal and solution structure of the Ca^{2+}-saturated protein and indicates that the hydrogen bonds between the two Ca^{2+}-binding loops are maintained in the absence of Ca^{2+}. The amide and C^α protons within this section of the peptide are some of the most downfield shifted, in accordance with previous studies of chemical shifts in an-

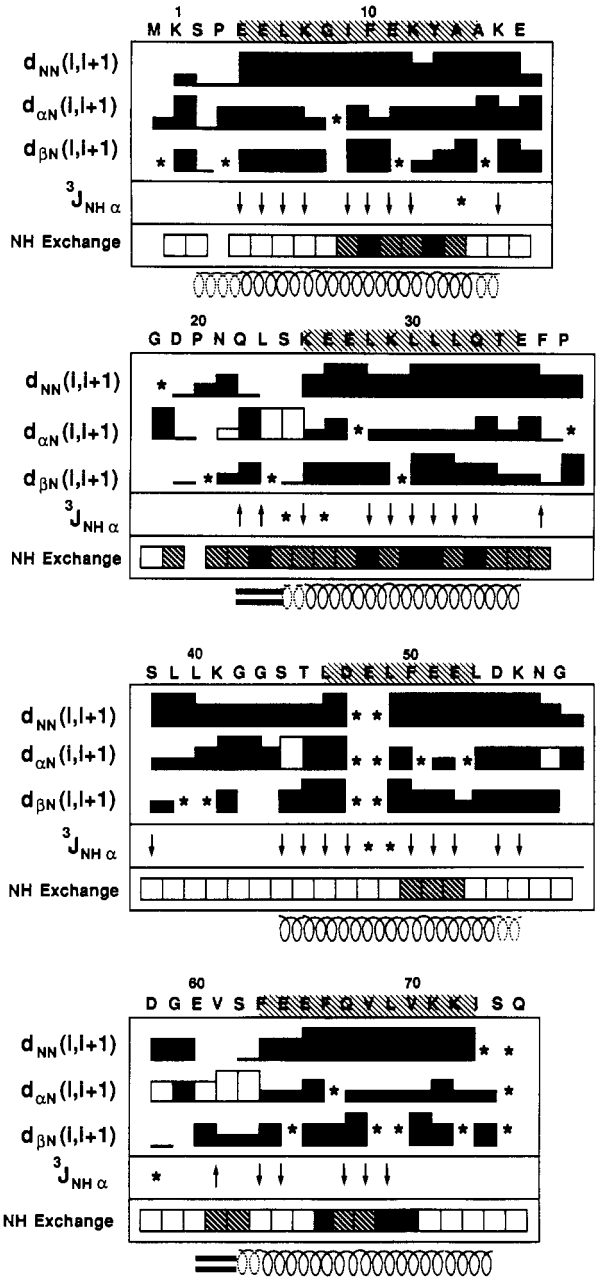

FIGURE 4: Summary of sequential NOE connectivities, backbone amide proton exchange rates, and backbone coupling constants ($^3J_{HN\alpha}$) observed in P43G and used to determine the elements of regular secondary structure. The one-letter code for the amino acid sequence is given at the top. The characteristic sequential NOE connectivities d_{NN}, $d_{\alpha N}$, and $d_{\beta N}$ are indicated by bars between the corresponding residues; the height of the bar gives a qualitative measure of the NOE intensity in a 200-ms NOESY experiment at pH 5.3. Filled bars were determined from a NOESY spectrum at 300 K, while the unfilled $d_{\alpha N}$ connectivities were obtained at 290 K from a NOESY with a jump–return observation pulse. NOEs to the prolines are to the C^{δ} protons rather than the backbone amide proton as discussed in Wüthrich et al. (1984). Connectivities that could not be identified due to resonance degeneracy are labeled with asterisks (*). Values of $^3J_{NH\alpha}$ are classified as small (<6 Hz) or large (>8 Hz) as indicated by ↓ or ↑, respectively. Slowly and very slowly exchanging backbone amide protons (see Materials and Methods) are shown by hatched squares and filled squares, respectively. The helices in the Ca^{2+}-saturated protein are indicated by shading around the amino acid sequence (Kördel et al., 1989). The location of secondary structure elements in the apo protein is marked by coils for helices and two parallel lines for the short antiparallel β-sheet. Fraying at the ends of the helices is indicated by a broken coil motif.

tiparallel β-sheets (Pardi et al., 1983).

Global Fold. Given the defined regions of secondary structure, and a number of readily identifiable long-range

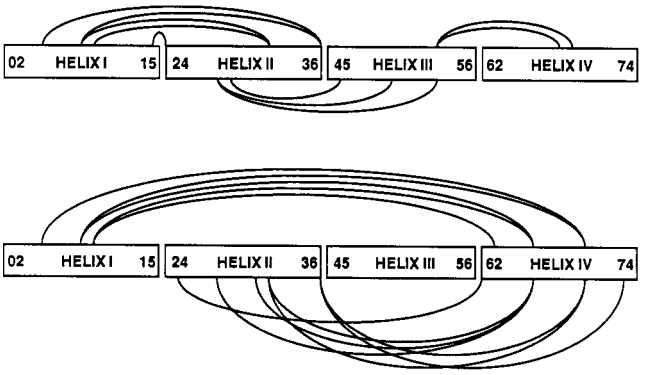

FIGURE 5: Interhelical NOEs observed in apo P43G. The horizontal boxes indicate the helical sections of the protein, the numbers inside the boxes defining the residues at the helix termini. (Top) NOEs between helices adjacent in the primary sequence. (Bottom) NOEs between helices nonadjacent in the primary sequence.

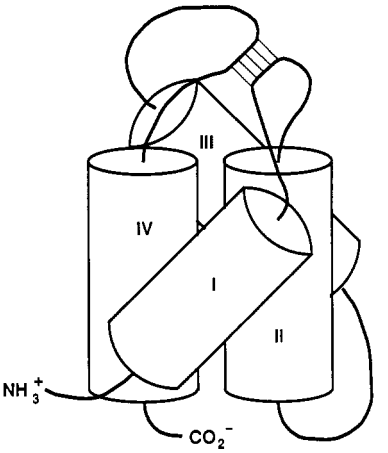

FIGURE 6: Schematic diagram of the global fold of apo P43G in solution. The four helical sections are depicted as cylinders and the remaining protein sections as thick lines. The position of the short β-sheet between the vacant Ca^{2+}-binding loops is indicated by the four parallel lines.

NOEs (Figure 5), it is possible to delineate the global fold of the backbone in schematic form (Figure 6). Contacts between the C-terminus of helix I and the N-terminus of helix II (Ala15 $C^{\alpha}H$–Pro20 $C^{\alpha}H$, Ala14 $C^{\alpha}H$–Leu23 $C^{\delta}H_3$) define a loop from Ala15 to Pro20/Leu23, this comprising the first metal-ion-binding region (free of Ca^{2+} in this instance). The constraints imposed by this loop and NOEs between Leu6 and Phe36 indicate roughtly antiparallel stacking of helix I with respect to II. The two metal-binding loops are brought into close proximity by the β-type interaction between Gln22–Ser24 and Glu60–Phe63. In addition, NOE contacts from Lys25 to Val61 and from Leu28 to Phe66 dictate a close approach of helix II and IV at their N-termini. Their C-termini are also in close proximity (NOEs are observed from Phe36 to Ile73), indicating a parallel stacking arrangement. NOEs are observed from the central and N-terminal portions of helix I to helix IV (Leu6 to Ile73 and Val70), suggesting that the packing of helix I and II may be skewed rather than perfectly antiparallel. At this stage of our analysis, relatively few long-range contacts to helix III have been assigned (Figure 5). No NOE contacts are observed between helix I and helix III. However, with the restraints imposed by the primary sequence, the well-defined orientation of helices II and IV, and these tertiary NOEs, the location of helix III is none-the-less fairly well defined. In summary, the global fold of apo calbindin maybe described as a central pair of helices (II and IV) separating two other helices (I and III), with each consecutive

Table I: ^{1}H NMR Chemical Shifts of Apo P43G Calbindin D_{9k} (pH 5.25, 300 K)[a]

residue	chemical shifts (ppm)					
	NH	C^α	C^β	C^γ	C^δ	other
M0		4.33	2.07, 2.50	2.28, (2.28)[b]		2.09 ($C^\epsilon H_3$)
K1	8.71	4.54	1.74, 1.88	1.37, 1.44	1.60, 1.67	2.87, 2.87 ($C^\epsilon H_2$)
S2	9.05	4.72	4.10, 4.47			
P3		4.22	2.16, 2.19	2.67, (2.67)[b]	3.99, 3.99	
E4	8.71	4.05	1.98, 2.10	2.30, 2.45		
E5	8.04	4.18	2.08, 2.43	2.31, 2.47		
L6	8.79	4.32	1.76, 2.32	1.98	0.90, 1.03	
K7	8.52	3.76	1.54, 1.82	0.79, (0.79)[b]	1.12, 1.23	2.62, 2.62 ($C^\epsilon H_2$)
G8	7.78	3.91, 3.97				
I9	7.91	3.93	2.18	1.25, 2.00	0.98	1.16 ($C^\gamma H_3$)
F10	8.61	3.56	2.94, 3.37			6.60, 7.08, 7.40 ($C^\delta H$, $C^\epsilon H$, $C^\zeta H$)
E11	8.69	3.93	2.08, 2.19	2.49, 2.68		
K12	7.65	3.90	1.91, 1.95	0.87, 1.30	1.54, 1.59	2.78, 2.78 ($C^\epsilon H_2$)
Y13	7.28	4.03	2.55, 2.78			7.55, 6.73 ($C^\delta H$, $C^\epsilon H$)
A14	8.46	3.96	0.77			
A15	7.38	4.01	1.42			
K16	7.12	3.88	1.85, 1.87	1.42, 1.58	1.66, 1.66	2.81, 2.86 ($C^\epsilon H_2$)
E17	7.30	4.47	2.01, 2.23	2.17, 2.24		
G18	8.32	3.71, 3.98				
D19	8.35	4.83	2.55, 2.82			
P20		4.43	2.02, 2.21	1.89, 2.02	3.86, (3.86)[b]	
N21	8.72	5.05	2.82, 2.99			8.00, 7.05 ($N^\delta H_2$)
Q22	7.70	5.14	1.76, 2.07	2.11, 2.24		6.58, 7.33 ($N^\epsilon H_2$)[c]
L23	8.92	4.88	1.36, 1.59	1.24	0.43, 0.45	
S24	8.35[d]	4.75	4.10, 4.38			
K25	8.76	3.68	1.49, 1.63	1.14, (1.14)[b]	1.53, 1.53	2.73, 2.76 ($C^\epsilon H_2$)
E26	8.46	3.94	1.97, 2.02	2.30, 2.36		
E27	7.72	4.08	2.02, 2.21	2.49, 2.55		
L28	8.71	4.00	1.43, 2.28	1.67	1.00, 1.11	
K29	8.24	3.75	1.80, 1.86	1.08, 1.39	1.52, 1.52	2.63, 2.66 ($C^\epsilon H_2$)
L30	7.35	4.12	1.76, 1.86	1.76	0.97, 1.04	
L31	8.31	2.89	0.98, 1.67	1.07	0.53, 0.93	
L32	8.82	4.01	1.40, 2.06	2.02	0.76, 0.83	
Q33	8.15	3.95	2.08, 2.25	2.38, 2.56		7.26, 6.81 ($N^\epsilon H_2$)
T34	7.82	4.08	4.29	1.25		
E35	8.83	4.24	1.56, 1.63	2.23, 2.51		
F36	7.81	5.16	2.98, 3.31			7.25, 7.15, 6.99 ($C^\delta H$, $C^\epsilon H$, $C^\zeta H$)
P37		4.31	2.00, 2.43	2.00, (2.00)[b]	3.25, 3.55	
S38	8.35	4.32	3.94, 4.03			
L39	7.94	4.37	1.66, 1.84	1.73	0.84, 0.84	
L40	7.63	4.40	1.65, 1.79	1.77	0.81, 0.94	
K41	7.89	4.35	1.80, 1.91	1.40, 1.47	1.67, 1.71	2.99, 3.01 ($C^\epsilon H_2$)
G42	8.27	3.98, 4.04				
G43	8.42	3.90, 4.16				
S44	8.27	4.63	3.92, 3.92			
T45	8.02	4.21	4.29	1.26		
L46	8.40	3.96	1.58, 1.63	1.54	0.83, 0.88	
D47	7.98	4.27	2.62, 2.69			
E48	7.96	4.05	2.05, 2.18	2.35, (2.35)[b]		
L49	7.97	4.07	1.48, 1.79	1.70	0.76, 0.78	
F50	8.48	4.12	3.17, 3.24			7.26, 7.20, 7.11 ($C^\delta H$, $C^\epsilon H$, $C^\zeta H$)
E51	7.98	4.12	2.17, 2.23	2.41, 2.52		
E52	7.65	4.07	2.16, 2.16	2.29, 2.42		
L53	7.72	4.16	1.46, 1.69	1.84	0.71, 0.79	
D54	8.10	4.52	2.53, 2.71			
K55	7.94	4.21	1.84, 1.89	1.45, 1.52	1.63, 1.66	2.97, 2.97 ($C^\epsilon H_2$)
N56	8.17	4.78	2.88, 2.93			7.73, 6.98 ($N^\delta H_2$)
G57	8.04	3.92, 4.05				
D58	8.49	4.74	2.81, 2.82			
G59	8.94	3.90, 4.05				
E60	7.86	4.93	1.83, 2.00	2.19, 2.35		
V61	9.18	4.65	2.29	0.96, 1.07		
S62	8.55	5.01	4.19, 4.52			
F63	9.34	3.47	2.22, 2.57			6.75, 7.16, 7.31 ($C^\delta H$, $C^\epsilon H$, $C^\zeta H$)
E64	8.69	3.73	1.91, 2.04	2.27, 2.39		
E65	7.56	4.01	2.04, 2.34	2.43, (2.43)[b]		
F66	8.76	4.13	3.23, 3.38			7.12, 7.33, 7.20 ($C^\delta H$, $C^\epsilon H$, $C^\zeta H$)
Q67	8.08	3.25	1.73, 1.76	1.67, 2.01		6.22, 6.71 ($N^\epsilon H_2$)
V68	7.12	3.43	2.16	0.87, 1.00		
L69	7.71	3.88	1.64, 1.74	1.67	0.82, 0.86	
V70	7.91	3.12	1.49	0.09, 0.46		
K71	7.53	3.91	1.81, 1.86	1.36, 1.48	1.61, 1.61	2.89, 2.89 ($C^\epsilon H_2$)
K72	7.68	4.06	1.92, 1.94	1.38, (1.38)[b]	1.58, 1.58	2.88, 2.88 ($C^\epsilon H_2$)
I73	7.57	4.29	2.01	1.23, 1.23	0.80	0.42 ($C^\gamma H_3$)
S74	7.61	4.51	3.85, 3.88			
Q75	7.60	4.14	1.94, 2.13	2.33, (2.33)[b]		6.80, 7.50 ($N^\epsilon H_2$)

[a] Chemical shifts are referenced to the H_2O signal at 4.75 ppm and are generally accurate to ±0.01 ppm (±0.03 ppm for geminal protons separated by <0.1 ppm). [b] Degeneracy assumed. [c] No intraresidue NOEs were observed to these two side-chain NH_2 groups. Assignment has been made on the basis of chemical shift comparisons with calcium-loaded protein. [d] NH resonance of S24 only observed in data acquired at 290 K.

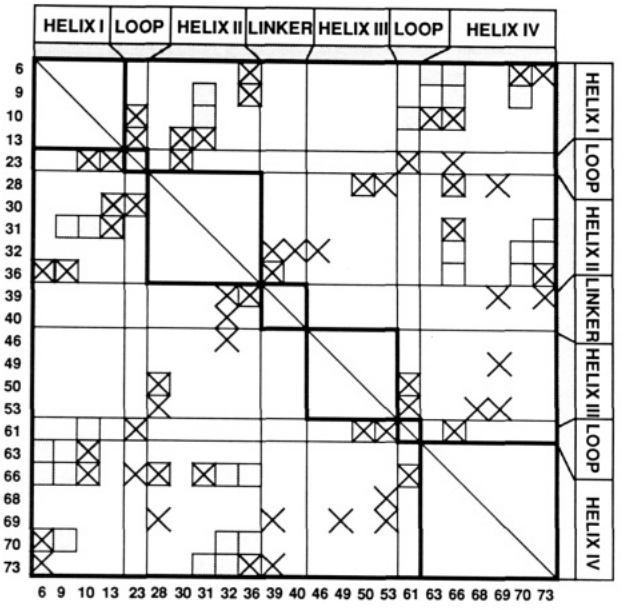

FIGURE 7: Comparison of the contacts between hydrophobic side chains in apo and Ca^{2+}-saturated calbindin D_{9k}. The protein is divided into seven segments: the four helices; the two Ca^{2+}-binding loops; the linker connecting the two EF hands. Each segment is proportional in length to the number of hydrophobic residues it contains, as indicated along the top and right side of the diagram. The sequence position of the hydrophobic residues is indicated along the bottom and left side of the diagram. A shaded square is drawn when at least one NOE is observed between side-chain protons of hydrophobic residues in different segments of the apo protein. A cross is drawn when side-chain carbon atoms of hydrophobic residues from two different segments are within 4.3 Å in the Ca^{2+}-saturated crystal structure of calbindin D_{9k} [adapted from Szebenyi and Moffat (1986)].

helix aligned in a roughly antiparallel manner (Figure 6).

Discussion

Using a range of 2D NMR experiments, it has been possible to assign the resonance positions of all nonexchangeable protons (with the exception of a few cases of unproven side-chain proton degeneracy), all backbone amide protons, and all but four resonances of exchangeable side-chain amide protons of apo calbindin D_{9k}. Complete resonance assignment provides the necessary background for identification of the regions of regular secondary structure within apo calbindin D_{9k}. Four helices and a short β-sheet between the metal-binding loops are found, as in the NMR (Kördel et al., 1989) and crystallographic (Szebenyi & Moffat, 1986) analyses of the Ca^{2+}-saturated protein. Characteristic (i,i+3) NOEs at the N-terminus of each helix (Ser2 $C^{\beta}H$–Glu5 NH, Ser24 $C^{\beta}H$–Glu27 NH, Thr45 $C^{\gamma}H_3$–Glu48 NH, and Ser62 $C^{\beta}H$–Glu65 NH) in both the apo and Ca^{2+}-saturated states are indicative of hydrogen bonds from $O^{\gamma}H$ of residue i to the backbone NH of residue $i + 3$ that stabilize the N-termini of the helices. These are also observed in the crystal structure (Szebenyi & Moffat, 1986). It is particularly interesting that the mini-β-sheet also remains intact in the absence of calcium ion despite the increase in the negative charge in the region of the Ca^{2+}-binding loops.

The elements of secondary structure and a few key long-range NOEs (Figure 5) provide the global folding pattern for the apo protein (Figure 6). At this relatively coarse resolution, the fold is highly similar to that obtained for the Ca^{2+}-saturated protein from NMR and crystallographic analyses. Although an exhaustive survey has yet to be carried out, there are a number of tertiary NOEs that are observed in both the apo and the Ca^{2+}-saturated protein, for example, the NOE from Tyr13 $C^{\epsilon}H$ to Glu35 $C^{\gamma}H_2$ that indicates the presence

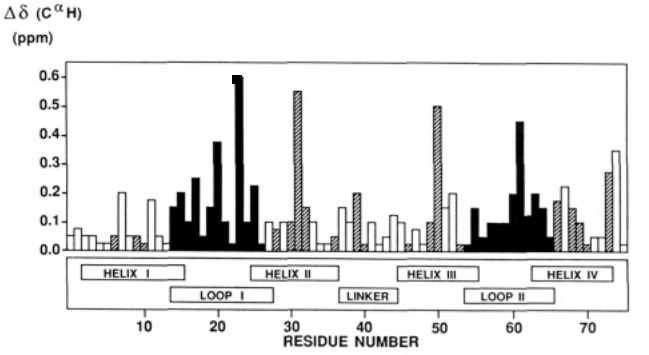

FIGURE 8: Chemical shift differences of the $C^{\alpha}H$ resonances in P43G in the Ca^{2+}-free and Ca^{2+}-saturated states. The sequence is displayed horizontally, the vertical bars indicating the absolute value of the chemical shift change. Filled bars indicate residues in the Ca^{2+}-binding loops, and striped bars indicate hydrophobic residues. The data for Ca^{2+}-saturated P43G are taken from Kördel et al. (1990).

of a hydrogen bond from the Tyr OH to the Glu carboxylate anion. Moreover, there is a strong correlation in the NOEs observed between hydrophobic residues in the apo protein and hydrophobic contacts present in the crystal structure of the Ca^{2+}-saturated protein, as shown in Figure 7.

Comparisons of the Ca^{2+}-free and Ca^{2+}-saturated domains of troponin C have resulted in the following predictions for the structural changes associated with Ca^{2+} chelation by EF-hand proteins: (1) changes in the conformation of the Ca^{2+}-binding loops, but with the mini-β-sheet remaining intact; (2) changes in the interhelix angles within each EF hand; (3) "changes in the relative disposition between the helix pairs I,IV and II,III" (Herzberg et al., 1986). Our results concerning the antiparallel β-sheet are fully consistent with this model, as are our observations that differences in sequential NOE intensities are localized to the Ca^{2+}-binding domains and the linker region. In the model, changes in the interhelix angles by the suggested 20°–40° would result in an increase in the separation of the helix axes by some 5–10 Å at their termini. Inspection of the long-range NOEs suggests that the changes in the relative orientation of the helices and the interhelix angles in calbindin D_{9k} are not as pronounced as those in the troponin C model.

Studies of the changes in secondary and tertiary structure of Ca^{2+}-binding regulatory proteins in response to titration with metal ions have been carried out with ^1H NMR chemical shift, CD, UV, and fluorescence [discussed in Skelton et al. (1990)]. Although some structural perturbations are associated with Ca^{2+} binding, these methods do not provide information concerning the magnitude or the exact nature of the conformational changes taking place. The problems associated with structural interpretations of ^1H NMR chemical shift changes are apparent from a plot of the differences in $C^{\alpha}H$ chemical shifts between apo and Ca^{2+}-saturated calbindin D_{9k} (Figure 8). Many residues undergo large changes as Ca^{2+} is bound (27 changing by more than 0.1 ppm), which could naively be associated with large structural reordering. However, the residues undergoing the largest changes as Ca^{2+} is bound are either hydrophobic or in the Ca^{2+}-binding loops. Chemical shift is very sensitive to changes in hydrogen bonding, ring current effects from carbonyl groups and aromatic rings, and through-bond electronic effects. Thus, even very modest differences in backbone conformation, aromatic side-chain positions in the hydrophobic core, or subtle reorganization of side chains in the Ca^{2+}-binding loops could give rise to the observed changes.

In contrast to our results which indicate that the conformations of Ca^{2+}-saturated and apo calbindin D_{9k} are not

greatly different, we find that removal of Ca^{2+} significantly alters the dynamics of the protein. Amide protons involved in secondary structure hydrogen bonds exchange when the hydrogen-bonding network is perturbed. The rate of amide proton exchange with solvent provides a means of probing the time scale on which proteins reorder themselves (Hvidt et al., 1966; Englander et al., 1972; Wagner, 1983b). Comparison of the rates in the Ca^{2+}-free and Ca^{2+}-saturated state shows that although the pattern of exchange rates versus sequence is not significantly altered by the Ca^{2+} content, the absolute values do change considerably. We find that the amide protons exchange between 2 and 3 orders of magnitude faster in the apo protein.[2] Furthermore, in the ^1H NMR studies on the Ca^{2+}-saturated protein (Kördel et al., 1989), it was noted that the C^δ protons of Phe10 were sufficiently broad at 300 K that no COSY correlations could be observed to $C^\epsilon H$. This was attributed to an intermediate (on the NMR time scale) 180° ring flip rate caused by the hydrophobic packing around the ring. In apo calbindin D_{9k}, no such resonance broadening is observed. Thus, both the amide exchange rates and the behavior of Phe10 indicate that removal of the calcium ions results in a greater degree of flexibility in the packing of its hydrophobic groups and in the hydrogen-bonding networks. These results are in accordance with thermal denaturation data: the Ca^{2+}-saturated protein is only 20% unfolded at 363 K, whereas the apo protein is 50% unfolded at this temperature (Wendt et al., 1988).

In summary, ^1H NMR data have been used to identify the elements of regular secondary structure and the global folding pattern of apo calbindin D_{9k}. Comparison with studies of the Ca^{2+}-saturated protein indicates that the changes in conformation produced by metal binding are small but that effects on the dynamics of the protein are substantial. More detailed structure calculations on apo and Ca^{2+}-saturated r-calbindin, based on NOE and torsion angle constraints, are in progress. These calculations, along with further studies of protein dynamics, will provide a more precise definition of the spatial relationships between the helices and the alteration of the side chains within the hydrophobic core and in the Ca^{2+}-binding loops.

ACKNOWLEDGMENTS

We thank Drs. Peter Brodin and Thomas Grundström for supplying protein pellets isolated from *E. coli*, Eva Thulin for purification of the samples, Johan Kördel, Mikael Akke, and Prof. Al Redfield for helpful discussions, and Dr. Mark Rance for continued support with experimental methods.

Registry No. Ca, 7440-70-2.

REFERENCES

Babu, Y. S., Bugg, C. E., & Cook, W. J. (1988) *J. Mol. Biol. 204*, 191–204.

Billeter, M., Braun, W., & Wüthrich, K. (1982) *J. Mol. Biol. 155*, 321–346.

Bodenhausen, G., Kogler, H., & Ernst, R. R. (1984) *J. Magn. Reson. 58*, 370–388.

Braunschweiler, L., Bodenhausen, G., & Ernst, R. R. (1983) *Mol. Phys. 48*, 535–560.

Brodin, P., Grundström, T., Hofmann, T., Drakenberg, T., Thulin, E., & Forsén, S. (1986) *Biochemistry 25*, 5371–5377.

Cavanagh, J., Chazin, W. J., & Rance, M. (1990) *J. Magn. Reson. 87*, 110–131.

[2] Similar results have been obtained in studies of amide proton exchange rates in wild-type calbindin D_{9k} (Linse et al., 1990).

Chazin, W. J., & Wright, P. E. (1987) *Biopolymers 25*, 973–977.

Chazin, W. J., & Wüthrich, K. (1987) *J. Magn. Reson. 72*, 358–363.

Chazin, W. J., Rance, M., & Wright, P. E. (1987) *FEBS Lett. 222*, 109–144.

Chazin, W. J., Rance, M., & Wright, P. E. (1988) *J. Mol. Biol. 202*, 603–622.

Chazin, W. J., Kördel, J., Drakenberg, T., Thulin, E., Brodin, P., Grundström, T., & Forsén, S. (1989a) *Proc. Natl. Acad. Sci. U.S.A. 86*, 2195–2198.

Chazin, W. J., Kördel, J., Drakenberg, T., Thulin, E., Hofmann, T., & Forsén, S. (1989b) *Biochemistry 28*, 8646–8653.

Cheung, W. Y. (1970) *Biochem. Biophys. Acta 532*, 373–375.

Chiba, K., & Mohri, T. (1987) *Biochemistry 26*, 711–715.

Chiba, K., Ohyashiki, T., & Mohri, T. (1983a) *J. Biochem. 93*, 487–493.

Chiba, K., Takeuchi, M., Ohyashiki, T., & Mohri, T. (1983b) *Chem. Pharm. Bull. 31*, 966–970.

Christakos, S., Gabrielides, C., & Rhoten, W. B. (1989) *Endocr. Rev. 10*, 3–26.

Dalgarno, D. C., Levine, B., Williams, R. J. P., Fullmer, C., & Wasserman, R. H. (1983) *Eur. J. Biochem. 137*, 523–529.

Davis, D. G. (1989) *J. Magn. Reson. 81*, 603–607.

Dorrington, K. J., Kells, D. I. C., Hitchman, A. J. W., Harrison, J. E., & Hofmann, T. (1978) *Can. J. Biochem. 56*, 492–499.

Drakenberg, T., Forsén, S., Thulin, E., & Vogel, H. J. (1987) *J. Biol. Chem. 262*, 672–678.

Ebashi, S., Kodama, A., & Ebashi, F. (1968) *J. Biochem. 64*, 465–477.

Englander, S. W., Downer, S. W., & Teitelbaum, H. (1972) *Annu. Rev. Biochem. 41*, 903–924.

Fujisawa, T., Ueki, T., & Iida, S. (1989) *J. Biochem. 105*, 377–383.

Fullmer, C. S., & Wasserman, R. H. (1981) *J. Biol. Chem. 256*, 5669–5674.

Heidorn, D. B., & Trewhella, J. (1988) *Biochemistry 27*, 909–915.

Hennessey, J. P., Parthasarathy, M., Johnson, W. C., Malencik, D. A., Anderson, S. R., Schimerlik, M. I., & Shalitin, Y. (1987) *Biopolymers 26*, 561–567.

Herzberg, O., & James, M. N. G. (1988) *J. Mol. Biol. 203*, 761–779.

Herzberg, O., Moult, J., & James, M. N. G. (1986) *J. Biol. Chem. 261*, 2638–2644.

Hofmann, T., Eng, S., Lilja, H., Drakenberg, T., Vogel, H. J., & Forsén, S. (1988) *Eur. J. Biochem. 172*, 307–313.

Hvidt, A., & Neilson, S. O. (1966) *Adv. Protein Chem. 21*, 287–386.

Ikura, M., Minowa, O., & Hikichi, K. (1985) *Biochemistry 24*, 4264–4269.

Ikura, M., Minowa, O., Yazawa, M., Yagi, K., & Hikichi, K. (1987) *FEBS Lett. 219*, 17–21.

Kakiuchi, S., & Yamazaki, R. (1970) *Biochim. Biophys. Acta 41*, 1104–1110.

Kataoka, M., Head, J. F., Seaton, B. A., & Engelman, D. M. (1989) *Proc. Natl. Acad. Sci. U.S.A. 86*, 6944–6948.

Kördel, J., Forsén, S., & Chazin, W. J. (1989) *Biochemistry 28*, 7065–7074.

Kördel, J., Forsén, S., & Chazin, W. J. (1990) *Biochemistry 29*, 4400–4409.

Kretsinger, R. H. (1972) *Nature (London), New Biol. 240*, 85–88.
Kretsinger, R. H. (1987) *Cold Spring Harbor Symp. Quant. Biol. 52*, 499–510.
Kumar, A., Ernst, R. R., & Wüthrich, K. (1980) *Biochem. Biophys. Res. Commun. 95*, 1–6.
Levitt, M., & Freeman, R. (1979) *J. Magn. Reson. 33*, 473–476.
Linse, S., Brodin, P., Drakenberg, T., Thulin, E., Sellers, P., Elmdén, K., Grundström, T., & Forsén, S. (1987) *Biochemistry 26*, 6723–6735.
Linse, S., Teleman, O., & Drakenberg, T. (1990) *Biochemistry* (in press).
Macura, A., & Ernst, R. R. (1980) *Mol. Phys. 41*, 95–117.
Marion, D., & Wüthrich, K. (1983) *Biochem. Biophys. Res. Commun. 113*, 967–974.
Moews, P. C., & Kretsinger, R. H. (1975) *J. Mol. Biol. 91*, 201–228.
Otting, G., Widmer, H., Wagner, G., & Wüthrich, K. (1987) *J. Magn. Reson. 66*, 187–193.
Pardi, A., Wagner, G., & Wüthrich, K. (1983) *Eur. J. Biochem. 137*, 445–454.
Plateau, P., & Guéron, M. (1982) *J. Am. Chem. Soc. 104*, 7130–7311.
Rance, M. (1987) *J. Magn. Reson. 74*, 557–564.
Rance, M., & Wright, P. E. (1986) *J. Magn. Reson. 66*, 372–378.
Rance, M., Sørensen, O. W., Bodenhausen, G., Wagner, G., Ernst, R. R., & Wüthrich, K. (1983) *Biochem. Biophys. Res. Commun. 131*, 1094–1102.
Rasmussen, H. (1986a) *N. Engl. J. Med. 314*, 1094–1101.
Rasmussen, H. (1986b) *N. Engl. J. Med. 314*, 1164–1170.
Rasmussen, H. (1989) *Sci. Am. 261* (4), 66–73.
Satyshur, K. A., Sambhorao, T. R., Pyzalska, D., Drendall, W., Greaser, M., & Sundaralingam, M. (1988) *J. Biol. Chem. 263*, 1628–1647.
Seamon, K. B., & Kretsinger, R. H. (1983) *Met. Ions Biol. 6*, 1–51.
Skelton, N. J., Kördel, J., Forsén, S., & Chazin, W. J. (1990) *J. Mol. Biol.* (in press).
Szebenyi, D. M. E., & Moffat, K. (1986) *J. Biol. Chem. 261*, 8761–8777.
Vogel, H. J., Drakenberg, T., Forsén, S., O'Neil, J. D., & Hofmann, T. (1985) *Biochemistry 24*, 3870–3876.
Wagner, G. (1983a) *J. Magn. Reson. 55*, 151–156.
Wagner, G. (1983b) *Q. Rev. Biophys. 16*, 1–57.
Wendt, B., Hofmann, T., Martin, S. R., Bayley, P., Brodin, P., Grundström, T., Thulin, E., Linse, S., & Forsén, S. (1988) *Eur. J. Biochem. 175*, 439–445.
Wüthrich, K. (1986) in *NMR of Proteins and Nucleic Acids*, Wiley, New York.
Wüthrich, K., Billeter, M., & Braun, W. (1984) *J. Mol. Biol. 180*, 715–740.

A Site-Directed Mutagenesis Study on *Escherichia coli* Inorganic Pyrophosphatase. Glutamic Acid-98 and Lysine-104 Are Important for Structural Integrity, whereas Aspartic Acids-97 and -102 Are Essential for Catalytic Activity†

Reijo Lahti,* Katariina Pohjanoksa, Taru Pitkäranta, Pirkko Heikinheimo, Tiina Salminen, Peter Meyer, and Jukka Heinonen

Department of Biochemistry, University of Turku, SF-20500 Turku, Finland

Received September 22, 1989; Revised Manuscript Received February 6, 1990

ABSTRACT: Analysis of the conservation of functional residues between yeast and *Escherichia coli* inorganic pyrophosphatases (PPases) suggested that Asp-97, Glu-98, Asp-102, and Lys-104 are important for the action of *E. coli* PPase [Lahti, R., Kolakowski, L. F., Heinonen, J., Vihinen, M., Pohjanoksa, K., & Cooperman, B. S. (1990) *Biochim. Biophys. Acta 1038*, 338–345]. We replaced these four residues by oligonucleotide-directed mutagenesis, giving variant PPases DV97, DE97, EV98, DV102, DE102, KI104, and KR104. PPase variants DV97, DV102, and KI104 had no enzyme activity, whereas PPase variants DE97, EV98, DE102, and KR104 had 22%, 33%, 3%, and 3% of the wild-type PPase activity, respectively. This suggests that Asp-97, Asp-102, and Lys-104 are essential for the catalytic activity of *E. coli* PPase. PPase variants DV98 and KR104 also had an increased sensitivity to heat denaturation; incubation of these mutant PPases at 75 °C for 15 min in the presence of 5 mM magnesium ion decreased the activity to 20% and 1%, respectively, of the initial value while 74% of the activity was observed with wild-type PPase. Furthermore, these thermolabile mutant PPases displayed the most profound conformational changes of the PPase variants examined, as demonstrated by the binding of the fluorescent dye Nile red that monitors the hydrophobicity of protein surfaces. Accordingly, Glu-98 and Lys-104 seem to be important for the structural integrity of *E. coli* PPase.

Inorganic pyrophosphatase (EC 3.6.1.1; PPase) catalyzes specifically the hydrolysis of inorganic pyrophosphate (PP_i) to two orthophosphates. This reaction plays an important role in energy metabolism, providing a thermodynamic pull for biosynthetic reactions, such as protein, RNA, and DNA synthesis (Kornberg, 1962; Peller, 1976; Lahti, 1983). PPases have been purified from a variety of sources primarily for kinetic (Josse, 1966a; Moe & Butler, 1972; Randahl, 1979;

† This work was supported by a grant from the city of Turku (Turun kaupungin apuraha).
* Address correspondence to this author.

0006-2960/90/0429-5761$02.50/0